

Phase Investigations Under Steam Oxidation Process at 800 °C for 1000 h of Advanced Steels and Ni-Based Alloys

T. Dudziak¹  · V. Deodeshmukh² · L. Backert³ ·
N. Sobczak¹ · M. Witkowska⁴ · W. Ratuszek⁴ ·
K. Chruściel⁴ · A. Zieliński⁵ · J. Sobczak¹ ·
G. Bruzda¹

Received: 4 May 2016 / Revised: 4 October 2016 / Published online: 2 November 2016
© The Author(s) 2016. This article is published with open access at Springerlink.com

Abstract The aim of this study was to investigate phase formation under steam oxidation conditions and steam oxidation behaviours of two solid-solution-strengthened alloys—HAYNES[®] 230[®] and 617 alloy—two gamma-prime (γ')-strengthened alloys—263 and HAYNES[®] 282[®]—and finally three austenitic steels rich in Cr—309S, 310S and HR3C. The samples were tested under 1 bar pressure in 100 % water–steam–water system at 800 °C for 1000 h. It was found that Ni-based solid-solution-strengthened alloys, HAYNES[®] 230[®] and 617 alloy, developed mainly Cr₂O₃ and MnCr₂O₄ phases on their surfaces, whereas the γ' -strengthened alloys, 263 and HAYNES[®] 282[®], formed Cr₂O₃, TiO₂ and MnTiO₃ phases, indicating slightly higher corrosion degradation rate. The austenitic steels exposed for 1000 h formed Cr₂O₃, Fe₃O₄ and MnCr₂O₄ with traces of Fe₃Mn(SiO)₄. Some sites on the austenitic steel surfaces were enriched with Fe₃O₄ with little amount of Cr. During the test, no spallation of the external oxide scale was observed. The kinetic data showed that only the 263 alloy oxidized according to parabolic behaviour, whereas the other alloys deviated from the parabolic rate law, with time exponents of 0.4–0.6 or 0.3. Finally, cross-sectioned investigations of the exposed samples revealed that Ni-based alloys underwent extended internal oxidation, with the highest extent in HAYNES[®] 282[®] reaching 25 μ m and the lowest in HAYNES[®]

✉ T. Dudziak
tomasz.dudziak@iod.krakow.pl

¹ Foundry Research Institute, Zakopianska 73, 30-418 Krakow, Poland

² Haynes International, 1020 West Park Avenue, Kokomo, IN 46904-9013, USA

³ Sandmeyer Steel Company, One Sandmeyer Lane, Philadelphia, PA 19116, USA

⁴ Faculty of Metals Engineering and Industrial Computer Science, AGH University Science and Technology, Al. A. Mickiewicza 30, 30-059 Krakow, Poland

⁵ Institute for Ferrous Metallurgy, K. Miarki 12-14, 44-100 Gliwice, Poland

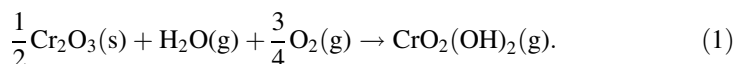
230[®] alloy reaching 7 μm . The austenitic steels showed no internal oxidation phenomena.

Keywords Steam oxidation · Oxidation kinetics · High temperature · XRD

Introduction

According to the International Energy Agency Energy Statistics, electricity and heat production accounts for 41 % of the total CO₂ emissions worldwide. Conventional solid fossil fuel power plants contribute significantly to CO₂ emissions and the European Union has put in place the legislation to reduce its emissions to 20 % below the 1990 levels by 2020 [1]. Reduction in CO₂ emissions from coal-fired power plants can be achieved by increasing the operating temperature and pressure of the steam cycle, which results in an increase in the overall plant efficiency. Increasing temperature along with pressure from 570 °C (38 % efficiency) to 760 °C increases the efficiency up to 55 % together with significant reduction in CO₂ emissions per kilowatt-hour-produced energy [2]. The energy sector is contributing to these goals by increasing the power generation efficiency; it is well known that the efficiency of electrical output is a function of temperature and pressure of the steam entering the steam turbine [3–5]. Generally, a 1 % increase in absolute efficiency results in as much as 3 % reduction in CO₂ emissions [6]. Hot sections of currently operating power plants (super heaters and re-heaters) use low or medium alloyed steels. However, such steels possess low corrosion resistance at a temperature range of 700–760 °C during which thick, non-protective scales with flaky, brittle structures susceptible to continuous scale spallation are formed, resulting in high metal loss and wall thinning and finally leading to the inability to withstand high steam pressures [7, 8].

In general, the materials containing up to 18 wt% Cr in the matrix, with the ability to form Cr₂O₃-rich scale, under long-term exposures and rich oxygen partial pressure conditions (steam–O₂, steam air), undergo catastrophic corrosion degradation attributed to chromia evaporation [9]. The process can be illustrated by the following reaction [10]:



The volatilisation of chromia scales leads to chromium depletion and therefore to the breakdown of the protective scales and an increase in the oxidation rate due to the nucleation of fast-growing iron-rich oxides [10]. In the literature, volatilisation has been reported to be less pronounced at low temperature [11]; however, above 700 °C, it is believed to influence the steam oxidation of the austenitic steels more significantly [12].

The formation of rich, stable, long-lasting chromia scale is essential for the high degree of performance in structural steels and Ni-based alloys. The study performed at 760 °C in 10 % water vapour and air-containing environments by Deodshmukh

[13] on HR-120[®], 18 wt% Cr 347HFG steel, HAYNES[®] 230[®], HAYNES[®] 282[®] Ni-based alloys showed that the surfaces were covered mainly by Cr₂O₃ and Fe₂O₃ phases in the case of 18 wt% Cr steel and Cr₂O₃ and in the case of high Cr Nickel-based alloy. In the case of HAYNES[®] 282[®] alloy, the scale was enriched with TiO₂ along with Cr₂O₃.

In a recent study, the high-temperature steam oxidation tests have been performed using a 100 % steam–water closed-loop system to investigate phase development and steam oxidation behaviour in pure water steam. In this work, Ni-based alloys, such as HAYNES[®] 230[®], 617 alloy, 263 alloy and HAYNES[®] 282[®], and highly alloyed steels with high concentration of Cr, such as 309S, 310S and HR3C, have been exposed to 800 °C for 1000 h. Microanalyses of the exposed alloys have been carried out using scanning electron microscope (SEM) in a backscattered electron (BSE) mode. Quantitative analysis of the chemical composition has been conducted using energy-dispersive X-ray spectroscopy (EDS) and X-ray diffraction (XRD) analyses using Bragg Brentano technique, and the grazing incidence of $\alpha = 1^\circ$ and $\alpha = 3^\circ$ has been carried out to study phase development.

Experimental Procedures

Steam Oxidation

The rig for high-temperature corrosion assessment of Ni-based and Fe-based alloys is shown in Fig. 1. The rig consists of heat resistant furnace, where reactive chamber made of stainless steel is inserted. Inside the stainless steel reactor, ceramic liner is placed. The liner prevents steam oxidation reaction from occurring in the stainless steel vessel; therefore, the liner is responsible for constant partial pressure of oxygen during high-temperature tests. Deionised water throughout the system of polyamide cables and stainless steel tubes is delivered by peristaltic pump to the system. Throughout the high-temperature tests, deionised water in the reservoir is constantly purged by nitrogen in order to eliminate oxygen dissolved in water from the ambient atmosphere (air). Nitrogen flow is constantly measured by flowmeter connected to the purging line. Prior to high temperature in the first instance, it is necessary to prepare the samples for the exposures. The samples are placed on the ceramic holder, and the holder with the samples is introduced to the furnace. The furnace is locked using four screws made of stainless steel. Further, when the chamber is closed, nitrogen is run in order to purge the chamber containing the samples for 2 h at 200 °C, to remove moisture and other impurities. At the same time, deionised water is constantly purged in the water tank. Finally, when temperature is increased to reach the final point, nitrogen is turned off and the peristaltic pump is turned on at 400 °C in order to deliver deionised water to the reactive chamber of the system. As mentioned, the tank with deionised water is constantly purged by nitrogen from the cylinder, and when the test is finished, during cooling period, the peristaltic pump needs to be turned off to prevent furnace inundation at around 200 °C. Further, the samples can be removed only when the furnace reaches room temperature (20 °C).

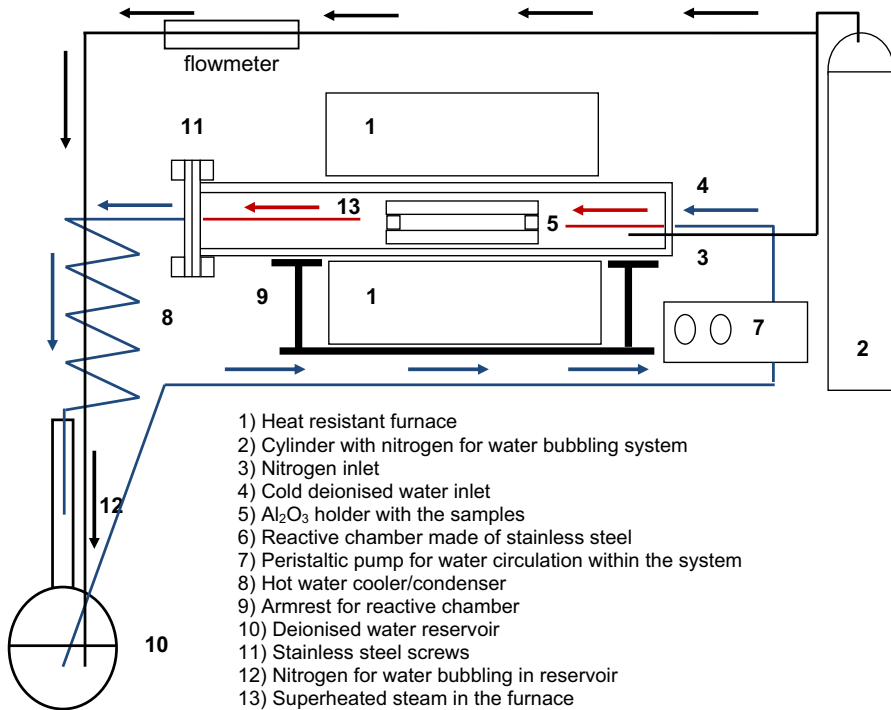


Fig. 1 Steam oxidation rig used in this study

XRD Investigations

XRD investigations were conducted by means of D500 Kristalloflex with monochromatic X-ray sources Cu ($\lambda K\alpha = 1.54\text{\AA}$) and EMPYREAN Panalytical with X-ray source Cu using Ni filter. The phase analyses have been performed using two techniques: Bragg–Brentano (BB) geometry and the geometry of constant angle called grazing incidence using $\alpha = 1^\circ$ and $\alpha = 3^\circ$. In BB geometry, the penetration depth of X-rays can be estimated using the following formula:

$$X = \frac{-\ln(1 - Gx)\sin\theta}{2\mu}, \quad (2)$$

where

- Gx denotes the intensity of the primary X-ray, giving important information related to irradiation volume and
- μ denotes the linear absorption coefficient.

In the grazing angle method, the penetration depth of X-rays was calculated using the following formula:

$$X = \frac{-\ln(1 - Gx)}{\left\{ \mu \left[\frac{1}{\sin \alpha} + \frac{1}{\sin(2\theta - \alpha)} \right] \right\}}, \quad (3)$$

where

- Gx denotes the intensity of the primary X-ray, giving important information related to irradiated volume; this value is equivalent to 0.95 (95 %);
- μ denotes the linear absorption coefficient and
- α denotes the incidence angle.

The calculated values of Gx with $Gx = 95\%$ taken as reference are shown in Table 1.

Materials

In the study, seven alloys were exposed to a temperature condition of 800 °C: two solid-solution-strengthened alloys, HAYNES[®] 230[®] and 617 alloy; two gamma-prime (γ')-strengthened materials, 263 alloy and HAYNES[®] 282[®] and high alloyed steels rich in Cr, 309S, 310S and HR3C. Table 2 shows the nominal compositions according to producer certificates of the Ni-based alloys and high alloyed steels, respectively. The materials prior to the steam test at 800 °C were cut out from the plate in small squares (20 mm²). The HR3C steel has been delivered in the form of tube section, the material was machined into tube segments, which had dimensions of ~15 mm length \times 10 mm width chord, with a 4-mm wall thickness. The surface of the steels and alloys was ground using 600 grid SiC paper. Furthermore, the samples were cleaned in acetone at 40 °C for 20 min in an ultrasonic bath. Prior and during the exposure, the samples were accurately weighed using a digital balance with a resolution of ± 0.01 mg for masses $m = < 80$ g. The digital balance Sartorius CPA225D was calibrated frequently using its internal calibration function and periodically with test weights.

Table 1 Penetration depth for the selected samples and the selected phases using two different geometries

Sample/phase	BB geometry (μm)	Grazing incidence $\alpha = 1^\circ$ (μm)	Grazing incidence $\alpha = 3^\circ$ (μm)
310S	2.89–7.32	0.29	0.84
263 alloy	3.91–9.91	0.39	1.14
HAYNES [®] 282 [®]	4.64–11.76	0.47	1.35
Cr ₂ O ₃	4.95–14.2	0.56	1.61
Cr ₃ O ₄	5.04–14.7	0.55	1.59

Table 2 Chemical composition of the materials (wt%) used in steam oxidation work

	Ni	Fe	Cr	Co	Mo	Si	Mn	Cu	Nb	La	Ti	Al	C	W	B	P	S	N
263 alloy	Bal.	0.6	20	20	6	0.4	0.6	0.2	-	-	1.2	0.6	0.06	-	-	-	-	-
617 alloy	Bal.	1	22	12.5	9	-	-	-	-	-	0.3	1.2	0.07	-	-	-	-	-
HAYNES® 230®	Bal.	3	22	5	2	0.4	0.5	-	-	0.02	-	0.3	0.1	14	0.015	-	-	-
HAYNES® 282®	Bal.	1.5	20	10	8.5	0.15	0.3	-	-	-	2.1	1.5	0.06	-	0.05	-	-	-
310S	21	Bal.	25	-	-	1.5	2	-	-	-	-	-	0.08	-	-	0.045	0.03	-
309S	14	Bal.	23	-	-	0.75	2	-	-	-	-	-	0.2	-	-	0.045	0.03	-
HR3C	20	Bal.	25	-	-	0.75	1.2	-	0.45	-	-	-	0.06	-	-	0.04	0.03	0.2

Results

Oxidation Behaviour

Figure 2 shows all the materials exposed in the study. The lowest weight gain under steam oxidation conditions has been observed in solid-solution-strengthened HAYNES[®] 230[®] alloy and the highest weight gain was observed in HAYNES[®] 282[®]. The weight gain of HAYNES[®] 282[®] was similar to 263 alloy, and the mass gain was moderate in 617 alloy. The weight gain of Ni-based samples exposed to steam oxidation were also very similar ranging from 0.37 mg/cm² (HAYNES[®] 230[®]) to 0.80 mg/cm² (HAYNES[®] 282[®]), respectively. The measured weight gain of 617 alloy after steam oxidation experiment showed the values similar to those of the advanced steels, where the highest weight gain was attributed to HR3C steel (0.56 mg/cm²), while 310S steel indicated the lowest value (0.50 mg/cm²), lower than for HAYNES[®] 282[®] and 263 Ni-based alloys.

From Figs. 3 and 4 where the exponent n factor for Fe- and Ni-based alloys has been calculated using log mass gain versus log time dependence, only the 263 alloy was found to oxidise under strict parabolic rate constant with $n = 0.5$ [14]. The other Ni-based alloys and advanced steels showed some incoherence in terms of parabolic mechanism, with n factor of 0.4–0.6. These deviations still could be considered close to the parabolic rate constant. However, HR3C steel showed exponent $n = 0.3$ indicating cubic time dependence law. According to Quadackers et al. [15], the process in most cases can be explained assuming that oxygen grain boundary diffusion is the dominating scale growth process in combination with an increase in oxide grain size with growth and perhaps with time.

Nevertheless, it has been found that advanced steels showed slightly better resistance to corrosion in terms of weight gain compared to those of γ' strengthened and solid-solution strengthened Ni-based alloys.

Furthermore, throughout the 1000-h test at 800 °C, no significant weight loss was observed. Therefore, chromia evaporation via the formation of CrO₂(OH)₂ phase

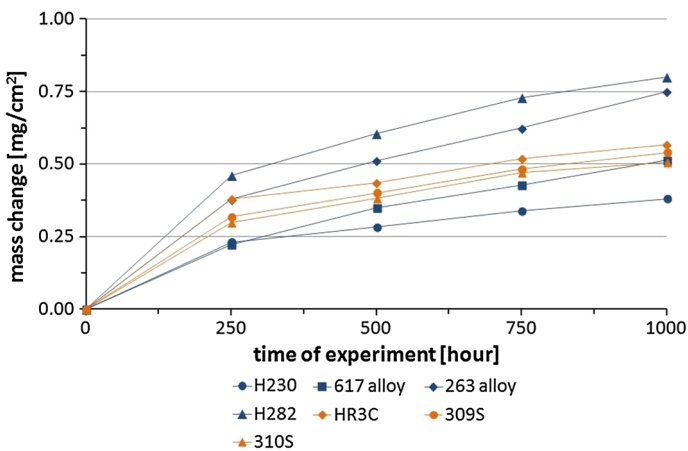


Fig. 2 Kinetic data of the materials exposed to steam oxidation regime at 800 °C for 1000 h

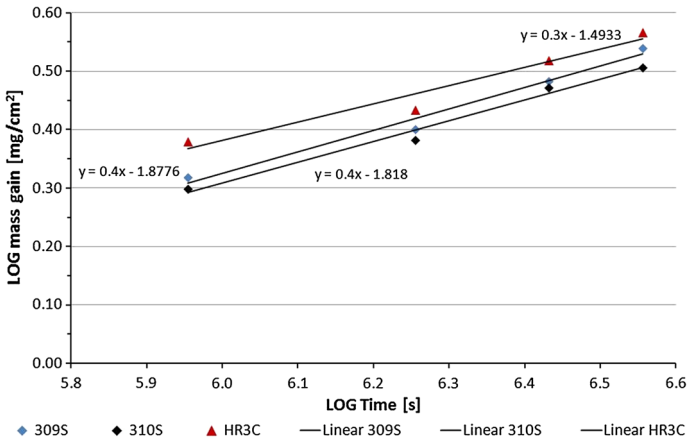


Fig. 3 A plot of log mass gain versus log time to determine the exponent n factor for Fe-based alloys

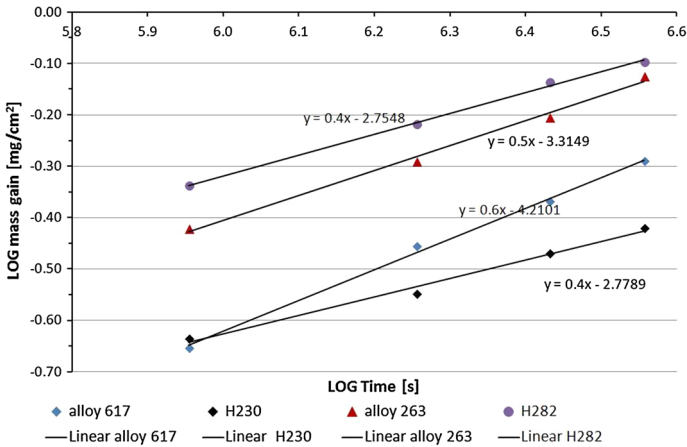


Fig. 4 A plot of log mass gain versus log time to determine the exponent n factor for Ni-based alloys

would not be considered in this study. Furthermore, according to Opila [16], in steam-rich atmospheres with a low oxygen partial pressure, there is minimal formation of the volatile Cr oxyhydroxide.

Microscopic Observations

Surface Morphologies

The surface microstructures of HAYNES[®] 230[®], 617 alloy, 263 alloy, HAYNES[®] 282[®], HR3C, 309S and 310S are shown in Fig. 5a–g, respectively. The surface microstructures of Ni-based alloys are shown in Fig. 5a–d. Generally, the exposed Ni-based alloy with no Ti addition (Table 2) developed MnCr₂O₄ and Cr₂O₃ oxides

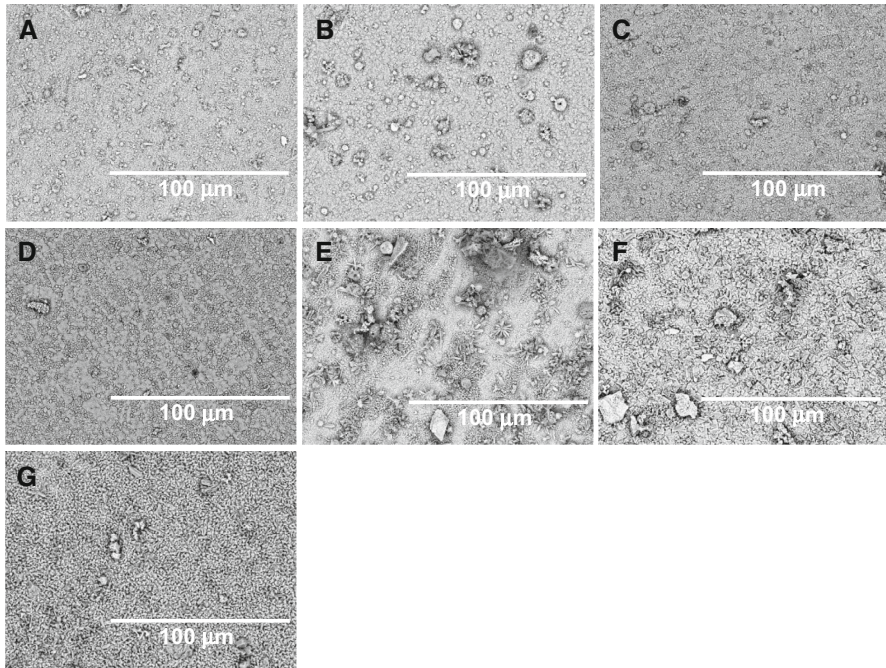


Fig. 5 Surface microstructures of the samples exposed to steam at 800 °C for 1000 h: **a** HAYNES[®] 230[®], **b** 617 alloy, **c** 263 alloy **d** HAYNES[®] 282[®], **e** HR3C, **f** 309S, **g** 310S

with chemical compositions of 40–50 wt% Cr, 36–40 wt% O and up to 10 wt% Mn, respectively. The Ni-based alloys containing Ti (Table 2) indicated Ti-rich oxide formation. The surface of HAYNES[®] 282[®] alloy showed 21 wt% Ti concentration, whereas 263 alloy contained approximately 14 wt% Ti. During the analyses, it was found that alloy rich in W (HAYNES[®] 230[®]) showed no W oxide formation. The analyses carried out on the Ni-based alloys, showed lack of Ni, suggesting the development of relatively dense, rich and protective scales.

The microstructures of the exposed stainless steels 309S, 310S and HR3C are shown in Fig. 5e–g. Similarly to Ni-based alloys, the steels developed adherent scales, rich in Cr (35–55 wt%), O (30–37 wt%) and Mn (6–17 wt%) suggesting the formation of spinel-like phases. The performed EDS analyses indicated the presence of Si on the exposed surfaces, suggesting the formation of Si-containing phases. The microstructures shown in Fig. 5e–g indicate that the surface of HR3C steel is covered unevenly by thick oxides, while 310S surface microstructure is rather smooth and consists of tiny crystals of the oxides developed under steam oxidation condition.

Phase Analyses

The performed XRD analyses carried out in this study allowed phase investigations of steam oxidised samples and a description of the phases formed on the surface.

The X-ray diffraction patterns were performed using 2θ from 17° to 125° where $\Delta 2 = 0.02^\circ$; however as shown in Fig. 6a–d, the analyses on the individual X-ray diffraction patterns for Ni-based alloys is presented from 20° to 80° omitting a high incidence angle, allowing better identification of the peaks of interest. In contrast to EDS analyses presented in paragraph 3.2.1, HAYNES[®] 230[®] (Fig. 6a) showed the presence of complex $\text{Co}_3\text{CrW}_3\text{C}$ carbide phases apart from MnCr_2O_4 , Cr_2O_3 and Cr_3O_4 . The carbide peak after 1000 h at 800°C was much weaker than that found in the substrate prior to the test. The carbide phase was possibly picked up from the substrate. The 263 alloy which contained Ti in the metal matrix (Fig. 6b) showed the development of an MnTiO_3 phase. The XRD diffraction patterns for 617 alloy and HAYNES[®] 282[®] are shown in Fig. 6c and d, respectively. It was found that 617 alloy indicated the development of $\text{Mo}_{17}\text{O}_{47}$ phase (MoxOy on XRD pattern), the oxide was found at 2θ of 22° on XRD; however, this position additionally identifies other oxides such as CoCr_2O_4 , FeCoCrO_4 , NiCr_2O_4 . The oxide $\text{Mo}_{17}\text{O}_{47}$ (MoxOy) and Cr_2O_3 showed the strongest signal due to the presence of large crystal size. In contrast, HAYNES[®] 282[®] alloy showed the development of MnTiO_3 , MnCr_2O_4 , Cr_2O_3 and TiO_2 phases, similar to 263 alloy, suggesting that addition of 1 wt% Ti to metal matrix initiates the formation of phases containing Ti and results in slightly higher mass gain than alloys without Ti addition (HAYNES[®] 230[®]).

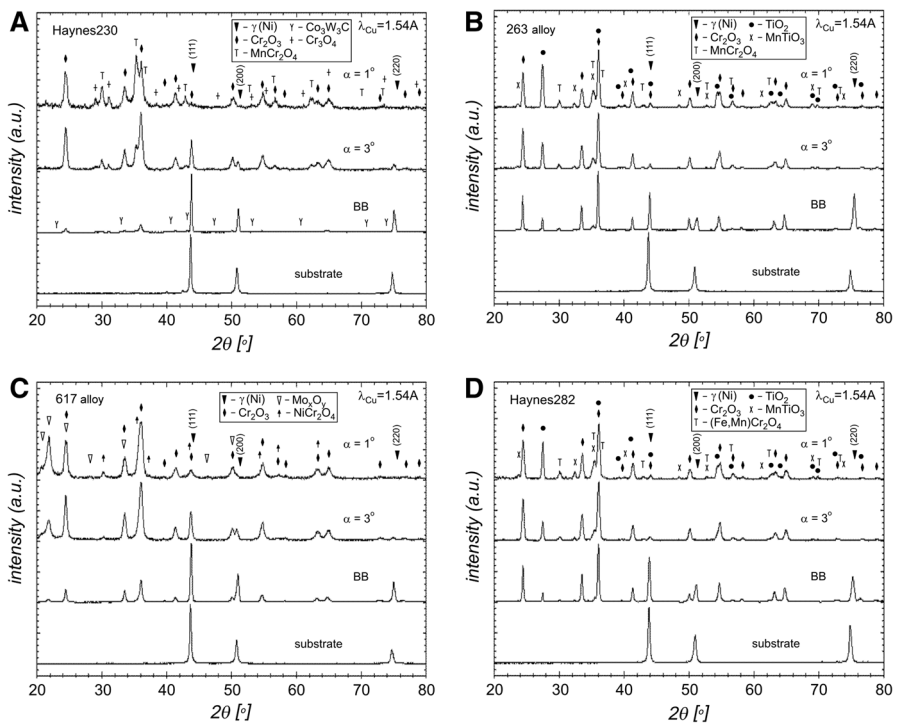
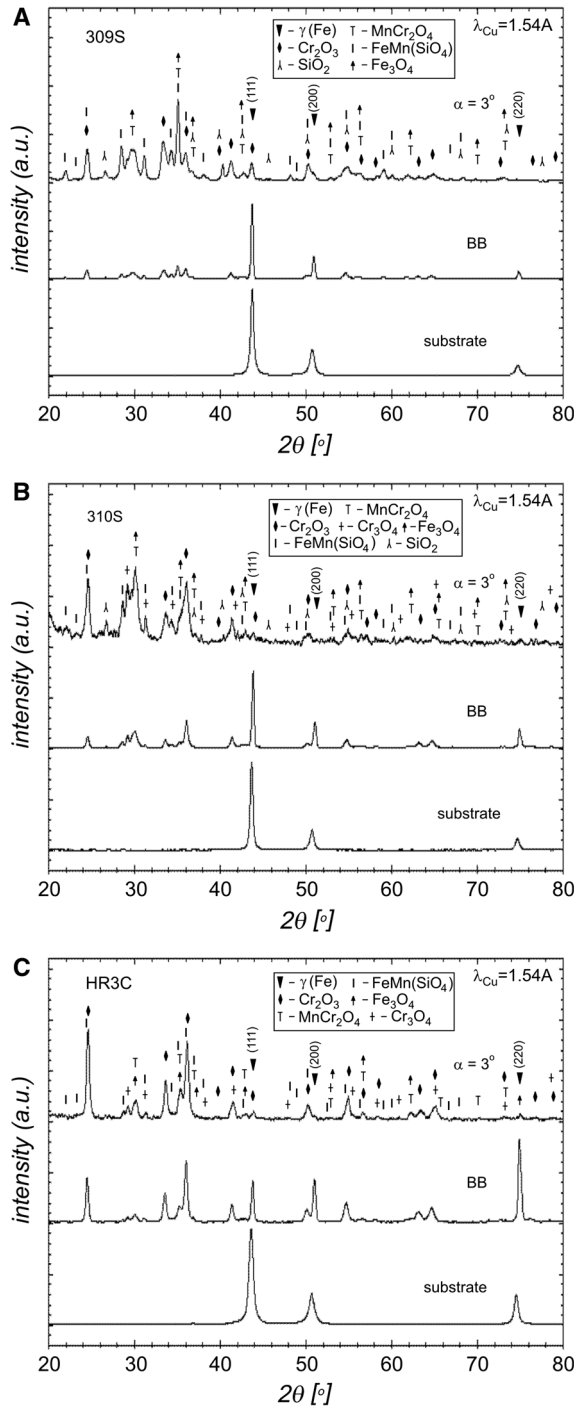


Fig. 6 XRD pattern for Ni-based alloys exposed to 800°C for 1000 h: **a** HAYNES[®] 230[®], **b** 263 alloy, **c** 617 alloy and **d** HAYNES[®] 282[®]

Fig. 7 XRD pattern of austenitic steels exposed to 800 °C for 1000 h: **a** 309S **b** 3110S and **c** HR3C



The XRD diffraction patterns for 309S, 310S and HR3C are presented in Fig. 7a–c, respectively. The EDS results have been confirmed by XRD, and the steels developed primarily are Cr_2O_3 , MnCr_2O_4 , Fe_3O_4 , Fe_2O_3 , SiO_2 and finally $\text{Fe,Mn}(\text{SiO}_4)$. However, the Si-containing phases were weaker much in comparison to Cr_2O_3 . Table 3 shows the list of phases identified on XRD investigations for Ni-based alloys and the advanced stainless steels.

Cross Sections

Figures 8 and 9 show the cross-sectional SEM images in BSE mode of the exposed Ni-based and Fe-based materials at 800 °C for 1000 h, respectively. Two solid-solution-strengthened alloys, HAYNES[®] 230[®] and 617 alloy; and two γ' -strengthened alloys, 263 and HAYNES[®] 282[®]; and high alloyed steels rich in Cr, 309S, 310S and HR3C, have been tested under 1 bar pressure in 100 % water–steam–water system. The microscopic observations performed on the cross-sectioned materials revealed that thin chromia scale rich in Cr_2O_3 and MnCr_2O_4 phases developed in HAYNES[®] 230[®] and 617 alloy, whereas HAYNES[®] 282[®] and 263 alloy developed thin oxide scale consisting of Cr_2O_3 , MnCr_2O_4 , MnTiO_3 and finally TiO_2 (based on XRD investigations).

Externally, the Ni-based alloys showed high degree of protectiveness; on the other hand, internally the same alloys underwent high degree of corrosion degradation due to internal oxidation after 1000 h exposure [17]. Among the exposed Ni-based alloys, the highest degree of internal oxidation penetration has been observed in the two γ' -strengthened alloys: 263 alloy and HAYNES[®] 282[®], where the penetration reached around 25 μm . The solid-solution-strengthened alloys showed slightly better resistance to internal oxidation process than that offered by γ' -strengthened alloys: the alloy 617 and HAYNES[®] 230[®] showed

Table 3 Phase developed under steam oxidation at 800 °C for 1000 h for Ni-based alloys and austenitic steels

Ni-based alloy	$\gamma(\text{Ni})$	Cr_2O_3	Cr_3O_4	MnCr_2O_4	TiO_2	MnTiO_3	Others	
HAYNES [®] 230 [®]	+	+	+	+			$\text{Co}_3\text{W}_3\text{C}$	
617 alloy	+	+	–	–	–	–	Mo_xO_y NiCr_2O_4	
263 alloy	+	+	–	+	+	+	–	
HAYNES [®] 282 [®]	+	+	–	+	+	+	FeCr_2O_4	
Austenitic steels	$\gamma(\text{Fe})$	Cr_2O_3	Cr_3O_4	MnCr_2O_4	FeCr_2O_4	$\text{FeMn}(\text{SiO}_4)$	SiO_2	Others
309S	+	+	–	+	–	+	+	$\text{Cr}_{1.3}\text{Fe}_{0.7}\text{O}_3$
310S	+	+	+	+	–	+	+	–
HR3C	+	+	+	+	–	+	+	$\text{Cr}_{1.3}\text{Fe}_{0.7}\text{O}_3$ Fe_3O_4

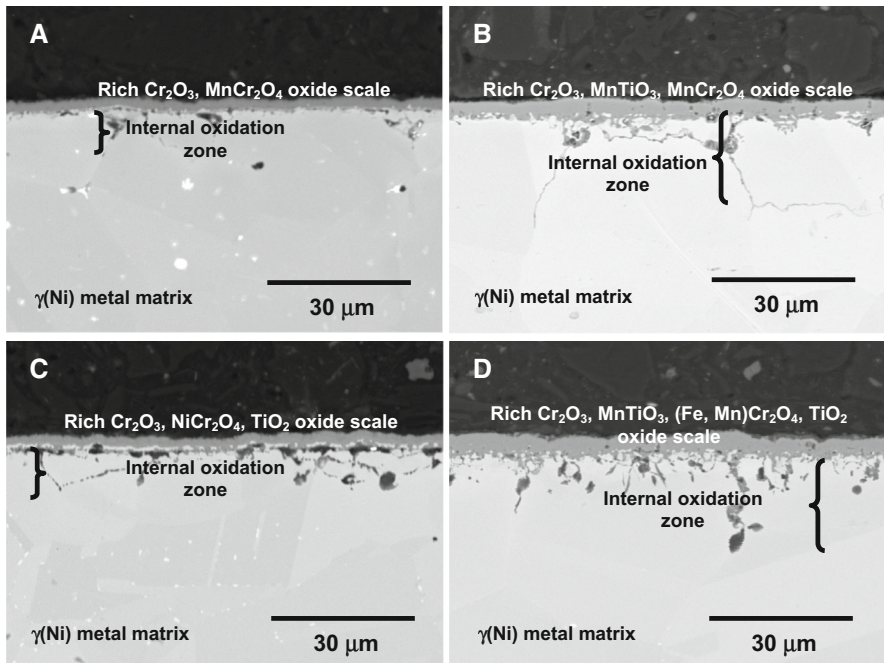
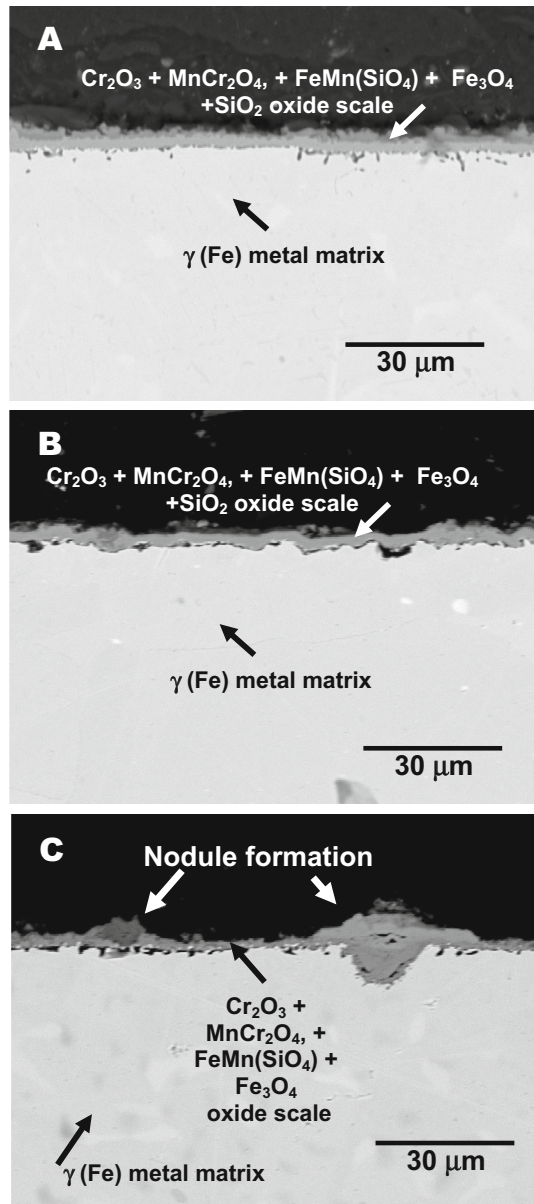


Fig. 8 Cross-sectional morphologies of the samples exposed to steam at 800 °C for 1000 h: **a** HAYNES[®] 230[®], **b** 617 alloy, **c** 263 alloy **d** HAYNES[®] 282[®]

internal oxidation process for around 8 and 7 μm, respectively. The calculations of internal oxidation depth (μm) versus Al + Ti content (wt%) in the Ni-based alloys are shown in Fig. 10. Essuman et al. [18] have shown that internal oxidation behaviour greatly varied with the Al + Ti content. In general, a similar trend was found in the work presented by Essuman et al. [18]. The alloys with low Al–Ti content (617 alloy, HAYNES[®] 230[®]) showed the formation of thinner external chromia scale after exposure to steam and less internal oxidation products. In contrast, in the alloys with higher Al–Ti contents (263 alloy, HAYNES[®] 282[®]), the thickness of the external chromia scale was higher and the internal oxidation too was higher. Based on the results, a strict comparison between these two studies cannot be performed, because Essuman et al. [18] performed the test at 800 °C under 17 bar pressure for 5000 h, whereas in this study the Ni-based alloys have been exposed to 800 °C for 1000 h.

The advanced steels exposed to 1 bar steam conditions at 800 °C for 1000 h, similarly to Ni based alloys showed thin oxide scale formation, with no internal oxidation zone formation. The steels with high Cr content showed the formation of thin oxide scale with thickness of only 2–3 μm. Some areas of the oxide scale have been covered by enriched Fe oxide [19]. The formation of Fe-rich oxide areas may predict about breakaway mechanism: the transition from protective oxidation, due to the exclusive formation of a Cr₂O₃ scale, to fast oxidation, characterised by the rapid growth of iron-rich oxides [20]. Nevertheless, the number of enriched areas

Fig. 9 Cross-sectional morphologies of the samples exposed to steam at 800 °C for 1000 h: **a** 309S **b** 310S and **c** HR3C



has been found to be relatively low as for the exposure duration at 800 °C. High corrosion resistance of advanced austenitic steels results from the formation of dense, adherent scale consisting of the following phases: MnCr_2O_4 , Cr_2O_3 mainly, spinel zone that has been observed underneath the Cr_2O_3 -rich oxide scale. The region in addition consisted of around 7 wt% Ni. Furthermore, the formation of

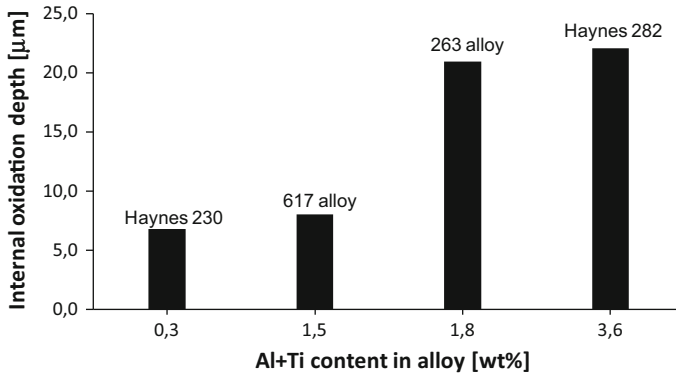


Fig. 10 Internal oxidation depth versus Al + Ti concentration (wt%) in Ni-based alloys

SiO₂ and other phases containing Si Si (Fe,Mn)SiO₄ in advanced steels is reported in this study as well.

Discussion

Ni-Based Alloys

Corrosion resistance of Ni-based alloys exposed to 800 °C for 1000 h is attributed mainly to the formation of rich Cr₂O₃ chromia scale. The highest performance was recorded in HAYNES[®] 230[®] alloy amongst the chromia formers in Ni-based alloys. In general, water steam is known to adversely affect the oxidation of chromia formers throughout:

- increased chromia growth from the doping of Cr₂O₃ with hydrogen species that leads to the oxidation reaction between the metal and H₂O [21],
- enhanced growth stresses that lead to scale spallation [22],
- enhanced internal oxidation of Cr by steam changing the solubility or diffusivity of oxygen in the alloy [22], leading to depletion of Cr reservoir from the deeper part of the metal matrix and inability to form long-lasting Cr₂O₃ scale.

In this study, extensive evaporation process was not found to occur throughout the whole 1000 h at 800 °C. The fact can be rationalised based on the work performed by Young et al. [23], where the evaporation process depends on oxygen delivered to the system, which therefore increases with the increasing pressure. Therefore, under 1 bar pressure at 800 °C, concentration of oxygen in steam is too low to conduct evaporation reaction (low partial pressure of oxygen). The process can start when much higher pressure is developed. Hence, long-lasting Cr₂O₃ scale developed as shown in this work is attributed to the low oxyhydroxide formation rate induced by a low oxygen partial pressure in steam under 1 bar pressure.

Holcomb and Alman [24] suggested that the alloys containing Ti and Mn reduce further the formation of volatile Cr oxyhydroxide from the scale due to the formation of outer layers of TiO_2 or Cr–Mn spinels. Sachitanand et al. [25] reported that higher Mn contents in the steel lead to lower Cr evaporation. When Mn content is high enough, lower Cr volatilisation is observed; nevertheless, higher Mn concentration in the oxide scale shows higher mass gain and the formation of thicker MnCr_2O_4 spinel layer. Holcomb et al. [26] found that Mn additions to Cr-rich Ni-based alloys decreases the activity of chromium within the oxide, either from solid-solution replacement of chromium with manganese (at low levels of manganese) or from the formation of manganese–chromium spinels (at high levels of manganese). This reduction in chromium activity leads to a predicted reduction in chromium evaporation by as much as a factor of 35 at 800 °C and 55 at 700 °C. Yang et al. [27] found that the additions of higher levels of Mn to the HAYNES[®] 230[®] facilitated the formation of a bi-layered oxide scale, where an outer consisted of M_3O_4 (M=Mn, Cr, Ni) spinel-rich layer at the oxide–gas interface over a Cr_2O_3 -rich sub-layer at the metal–oxide interface. Deodeshumkh [13] found the beneficial effects of Mn in HAYNES[®] 230[®] and alloy X where a thin layer of MnCr_2O_4 developed.

The results obtained in this work clearly indicate that Cr evaporation has not occurred in large extent, for evidence; the 617 alloy with no Mn addition showed similar high temperature behaviour under steam oxidation condition as the alloys with Mn addition, however the effect cannot be completely refused.

In general, two solid-solution-strengthened alloys, HAYNES[®] 230[®] and 617 alloy, showed lower weight gain than two γ' -strengthened alloys, 263 and HAYNES[®] 282[®]. It is believed that higher mass gain for γ' -strengthened alloys occurred due to the development of a TiO_2 phase on the surface. It is well known that the TiO_2 phase possesses a high number of defects in the crystal structure and is often responsible for accelerated mass gain in TiAl alloys [28, 29]. Karake et al. [30] indicated that the doubly ionised oxygen vacancies are responsible for the kinetic growth rate of TiO_2 scales over Ti-rich alloy and accelerated weight gain.

Similar to the results obtained in this work, the study carried out by Cruchley et al. [31] showed that the growth rate of the chromia layer is significantly greater than that observed in Ti-free samples. The accelerated oxidation rate in HAYNES[®] 282[®] as argued by Cruchley et al. [31] is attributed to the increased ionic transport caused by doping of the chromia layer by titanium and creation of vacancies on the chromium sub-lattice. In the past, the effect of Ti in Ni-based alloys with the addition of Ti has been shown by Chen et al. [32], Kim et al. [33] and recently by Taylor et al. [34]. Furthermore, it has been found that Ti has negative effect on chromia scale due to the formation of higher number of chromium vacancies directly inducing higher diffusion rates of the chromium ion through the oxide scale. However, concentration of Ti in the chromia scale is likely to reduce due to oxide scale thickening and depletion of Ti in the alloy.

The exposed Ni-based alloys as shown underwent different degrees of internal oxidation phenomena. The lowest degree was in HAYNES[®] 230[®], where the effect of as little as 0.02 wt% addition of La is observed on improvement in scale adhesion and lower internal oxidation zone formation at higher temperature as reported in a

study by Yang et al. [35]. Other Ni-based alloys exposed in this study internally oxidised much more severely than HAYNES[®] 230[®].

It has been found that the highest degree of internal oxidation process corresponds to the Ni-based alloy with the highest Ti concentration in the metal matrix (HAYNES[®] 282[®]). Therefore, it can be suggested, based on the experimental data achieved in the study, that the presence of Ti in the metal matrix highly enhanced the susceptibility to internal oxidation process at high temperatures in steam environment.

The process is driven by the ability of Ti and Al to oxidation reaction due to high negativity of Gibbs free energy formation (Table 4). In comparison to the other elements (Si, Ni, Cr, Mn), the formation of TiO₂ and Al₂O₃ requires as low as ΔG_T^O of -749.6 and -892.2 kJ·mol⁻¹ energy to form the oxide. However, the concentration of Al in the HAYNES[®] 282[®] alloy is much lower compared to Ti concentration, indicating that the formation of TiO₂ prevailed much more than Al₂O₃.

In the other Ni-based alloys, 617 alloy and 263 alloy, the concentration of Al and Ti is more balanced than that in HAYNES[®] 282[®]; thus, a lower degree of internal oxidation process has been found. In HAYNES[®] 230[®] alloy in comparison to the other Ni-based alloys, the absence of Ti in the metal matrix and relatively low Al concentration result in limited internal oxidation process.

Austenitic Steels

The advanced steels rich in Cr and with tiny Si concentration, in comparison to Ni-based alloys, showed slightly better corrosion resistance in terms of weight gain; furthermore, the steels show no internal oxidation zone formation at 800 °C. The observed corrosion resistance is attributed to the formation of rich Cr₂O₃ and MnCr₂O₃. The role of these oxides in high-temperature corrosion has been discussed previously by many researchers [2, 7, 36, 37]. Henry et al. [38] have shown that increased Si content from 0 to 1 wt% delays breakaway oxidation mechanism i.e. in 15 wt% Cr steel, 1 wt% Si addition delays breakaway oxidation from 2 to more than 50 h. Similarly, addition of Si to 309S and 310S steels (>20 wt% Cr) may further enhance the breakaway process, not only because of high Cr content and high activity of Cr₂O₃, but also due to the effect of Si.

Table 4 Gibbs energy of formation of metal oxides at 800 °C

Phase	Al ₂ O ₃ (KJ·mol ⁻¹)	TiO ₂ (KJ·mol ⁻¹)	SiO ₂ (KJ·mol ⁻¹)	MnO (KJ·mol ⁻¹)	Cr ₂ O ₃ (KJ·mol ⁻¹)
ΔG_T^O	-892.2	-749.6	-718.5	618.0	-566.9
Phase	MoO ₂	CoO	NiO	Mn ₃ O ₄	MoO ₃
ΔG_T^O	-434.4	-320.7	-287.1	-201.0	-173.1
Phase	Co ₃ O ₄				
ΔG_T^O	-60.1				

The exposed steels show lack of evaporation of Cr from Cr_2O_3 phase due to the formation of $\text{CrO}_2(\text{OH})_2$ (g) phase, similar to Ni-based alloys. Lack of evaporation process in steels similar to Ni-based alloys is due to the formation of MnCr_2O_4 phase as mentioned previously. The beneficial effect of MnCr_2O_4 formation in advanced steels can be observed in this work. Two steels 309S and 310S with higher concentration of Mn than that in HR3C showed lower weight gain. Furthermore, the HR3C steel with as high as 25 wt% Cr and lower concentration of Mn underwent higher degradation rate related to the formation of Fe-rich area. The rich Fe_3O_4 area was found to be distributed on the oxidised surface. The formation of such microstructures may indicate the initiation of the breakaway oxidation in elongated exposures [39].

Ennis et al. [40] have found that oxide scales formed on ferritic and austenitic steels change in the following manner with the increasing Cr content: from haematite/magnetite to magnetite/(Fe, Cr) $_3\text{O}_4$ spinel to (Fe, Cr) $_3\text{O}_4$, spinel/ Cr_2O_3 and finally to a pure Cr_2O_3 . A ranking of alloys in terms of steam oxidation resistance has been proposed (least to the most resistant): T23, T91, T92, Super 304H, T347HFG, HR3C, HR6 W, HR120, Alloy 230 and Inconel 740. However, the results clearly indicate that even 23–25 wt% Cr is not sufficient to develop Cr_2O_3 oxide scale exclusively, where Cr_2O_3 and MnCr_2O_4 phases predominantly formed with trace amounts of Fe, Mn(SiO_4) and SiO_2 .

Conclusions

The aim of this paper was to show the phase development of and influence of 100 % steam environment on Ni-based alloys and high alloyed austenitic steels: solid-solution-strengthened materials, 617 alloy and HAYNES[®] 230[®], and γ' -strengthened alloys, 263 and HAYNES[®] 282[®]. Based on the results obtained in this study, the following conclusions can be made:

- All of the exposed high alloyed steels and Ni-based alloys showed low weight gain at 800 °C for 1000 h.
- Only the 263 alloy presented strict parabolic behaviour.
- Alloys 617, HAYNES[®] 282[®], HAYNES[®] 230[®] and 309S, 310S steels showed close parabolic rate.
- The HR3C steel indicated cubic rate constant with an n factor of 0.3.
- No evaporation process $\text{CrO}_2(\text{OH})_2$ (g) phase was observed.
- Ni-based alloys showed the following phases on XRD investigations:
 - 6 HAYNES[®] 230[®]: Cr_2O_3 , MnCr_2O_4 and Cr_2O_3
 - 263 alloy: Cr_2O_3 , MnTiO_3 , MnCr_2O_4 and TiO_2
 - 617 alloy: Cr_2O_3 , NiCr_2O_4
 - HAYNES[®] 282[®]: Cr_2O_3 , MnTiO_3 , MnCr_2O_4 and TiO_2

- The Ni-based alloys containing Ti showed higher weight gain kinetics due to Ti doping effect in contrast to the alloys with no Ti in the matrix, i.e. HAYNES[®] 230[®].
- The Ni-based alloy with the highest Ti concentration showed the highest rate of internal oxidation process, with the highest rate noted in HAYNES[®] 282[®] and the lowest rate in HAYNES[®] 230[®].
- There is a strong correlation between Ti concentration and internal oxidation process
- No strict evidence for Mn effect was found as mentioned by several authors [13, 26, 27]
- Fe-based materials showed the development of the following phases on XRD investigations:
 - 309S: Cr₂O₃, MnCr₂O₄, γ(Fe), SiO₂, Fe,Mn(SiO)₄
 - 310S: Cr₂O₃, MnCr₂O₄, γ(Fe), SiO₂
 - HR3C: Cr₂O₃, MnCr₂O₄, γ(Fe), Fe₃O₄, Fe,Mn(SiO)₄ (traces)
- Internal oxidation process has not been found in Fe-based alloys at 800 °C after 1000 h steam oxidation

Acknowledgments The authors would like to acknowledge National Science Centre in Poland for the financial support of the fundamental research under the project number 2014/13/D/ST8/03256. Furthermore, the authors would like to acknowledge the following materials providers: Haynes International, Sandmeyer Steel Company and finally Institute for Ferrous Metallurgy in Poland for Ni based and advanced steels supply.

Open Access This article is distributed under the terms of the Creative Commons Attribution 4.0 International License (<http://creativecommons.org/licenses/by/4.0/>), which permits unrestricted use, distribution, and reproduction in any medium, provided you give appropriate credit to the original author(s) and the source, provide a link to the Creative Commons license, and indicate if changes were made.

References

1. Smarter, greener, more inclusive? Indicators to support the Europe 2020 strategy, Eurostat, Statistical books, Luxembourg: Publications Office of the European Union, (2015) ISSN 2363-2208
2. R. Viswanathan, J. Sarver and J. M. Tanzosh, *Journal of Materials Engineering Performance* **15**, 255 (2006).
3. N. Komai, F. Masuyama and M. Igarashi, *Journal of Pressure Vessel Technology* **127**, 190 (2005).
4. J. Gabrel, C. Coussement, L. Verelst, R. Blum, Q. Chen and C. Testani, *Materials Science Forum* **369–372**, 931 (2001).
5. W. J. Quadackers, P. Ennis, J. Zurek and M. Michalik, *Materials at High Temperatures* **22**, 27 (2005).
6. K. Burnard, J. Jiang, B. Li, G. Brunet and F. Bauer, *Emissions Reduction through upgrade of Coal-Fired power plants-learning from Chinese Experience*, (International Energy Agency (IEA), Masdar, 2014).

7. I. Wright, A. Sabau and R. Dooley, *Materials Science Forum* **595–598**, 387 (2008).
8. I. G. Wright, P. J. Maziasz, F. V. Ellis, T. B. Gibbons and D. A. Woodford, *Materials Issues for turbines for operation in ultra-supercritical steam*, 29th International Technical Conference on Coal Utilization and fuel systems, Clearwater, Florida (2004).
9. H. Asteman, J. E. Svensson, L. G. Johansson and M. Norell, *Oxidation of Metals* **52**, (1/2), 95 (1999).
10. D. J. Young, *Materials Science Forum* **595–598**, 1189 (2008).
11. H. Asteman, J. E. Svensson, M. Norell and L. G. Johansson, *Oxidation of Metals* **54**, (1/2), 11 (2000).
12. M. Lukaszewicz, N. J. Simms, T. Dudziak and J. R. Nicholls, *Oxidation of Metals* **79**, (5–6), 473 (2013).
13. V. P. Deodshumukh, *Oxidation of Metals* **79**, 567 (2013).
14. B. Pieraggi, *Oxidation of Metals* **27**, (3), 177 (1986).
15. W. J. Quadakkers, D. Naumenko and E. Wessel, *Oxidation of Metals* **61**, (1/2), 17 (2004).
16. E. J. Opila, *Materials Science Forum* **461–464**, 765 (2004).
17. D. J. Young, *High Temperature Oxidation and Corrosion of Metals, Chapter 6 Alloy Oxidation II: Internal Oxidation*, Elsevier 2016.
18. E. Essuman, L. R. Walker, P. J. Maziasz and B. A. Pint, *Materials Science and Technology* **29**, (7), 822 (2013). doi:[10.1179/1743284712Y.0000000103](https://doi.org/10.1179/1743284712Y.0000000103).
19. P. Tomaszewicz and G. R. Wailwork, *Oxidation of Metals* **19**, (5/6), 165 (1983).
20. T. Gheno, D. Monceau and D. J. Young, *Corrosion Science* **77**, 246 (2013).
21. T. Norby, *Journal de Physique IV* **3**, 99 (1993).
22. E. Essuman, G. H. Meier, J. Żurek, M. Hänsel and W. J. Quadakkers, *Oxidation of Metals* **69**, (3/4), 143 (2008).
23. D. J. Young and B. A. Pint, *Oxidation of Metals* **66**, (3/4), 137 (2006).
24. G. R. Holcomb and D. E. Alman, *Scripta Materialia* **2006**, 54 (1821).
25. R. Sachitanand, M. Sattari, J.-E. Svensson and J. Froitzheim, *International Journal of Hydrogen Energy* **38**, 15328 (2013).
26. G. R. Holcomb and D. E. Alman, *The Effect of Manganese Additions on the Reactive Evaporation of Chromium in Ni–Cr Alloys*, (Albany Research Center, New York, 2006).
27. Z. G. Yang, G. G. Xia, J. W. Stevenson and P. Singh, *Observations on the Oxidation of Mn-Modified Ni-Base Haynes 230 Alloy Under SOFC Exposure Conditions*, (PNNL-15304, Richland, 2005).
28. T. S. Bjørheim, A. Kuwabara and T. Norby, *The Journal of Physical Chemistry C* **117**, (11), 5919 (2013).
29. H. L. Du, P. K. Datta, Z. Klusek and J. S. Burnell-Gray, *Oxidation of Metals* **62**, (3), 178 (2004).
30. S. A. Karake and P. B. Aswath, *Journal of Materials Science* **32**, 2845 (1997).
31. S. Cruchley, H. E. Evans, M. P. Taylor, M. C. Hardy and S. Stekovic, *Corrosion Science* **75**, 58 (2013).
32. J. Chen, P. Rogers and J. A. Little, *Oxidation of Metals* **47**, 381 (1997).
33. D. Kim, C. Jang and W. Ryu, *Oxidation of Metals* **71**, 271 (2009).
34. M. P. Taylor, H. E. Evans, S. Stekovic and M. C. Hardy, *Materials High Temperature* **29**, 45 (2012).
35. Z. G. Yang, G. G. Xia, J. W. Stevenson and P. Singh, *Observations on the Oxidation of Mn-Modified Ni-Base Haynes 230 Alloy Under SOFC Exposure Conditions (No. PNNL-15304)*, (PNNL, Richland, 2005).
36. A. Fry, S. Osgerby and M. Wright, *Oxidation of Alloys in Steam Environments: A Review*, (NPL, United Kingdom, 2002).
37. N. K. Othman, N. Othman, J. Zhang and D. J. Young, *Corrosion Science* **51**, 3039 (2009).
38. S. Henry, A. Galerie and L. Antoni, *Materials Science Forum* **369–372**, 353 (2001).
39. H. E. Evans, A. T. Donaldson and T. C. Gilmour, *Oxidation of Metals* **52**, 379 (1999).
40. P. Ennis and W. Quadakkers, *International Journal of Pressure Vessels and Piping* **84**, 82 (2007).